energies

MDPI

Article

Simulations of Airflow in the Roof Space of a Gothic Sanctuary Using CFD Models

Radoslav Ponechal, Peter Krušinský *, Peter Kysela and Peter Pisca

Department of Building Engineering and Urban Planning, Faculty of Civil Engineering, University of Zilina, 010 26 Zilina, Slovakia; radoslav.ponechal@uniza.sk (R.P.); kysela11@uniza.sk (P.K.); peter.pisca@uniza.sk (P.P.)
* Correspondence: peter.krusinsky@uniza.sk (P.K); Tel.: +421-41-513-5707

Abstract: For a deep understanding of the airflow in an environment of historic wooden trusses, it is necessary to analyze the object using simulation methods. To calculate the amount of air passing through the structural openings (components) using dynamic simulation, multi-zone network models based on the simplicity of modeling the individual zones are suitable. For a more detailed analysis of airflow and temperature distribution within one space, a computational fluid dynamics (CFD) simulation model was performed. The air volume through openings and surface temperatures was adopted from the multi-zone airflow network model. By using this simulation technique during a sunny summer day four characteristic states of air movement were simulated in the attic: more intense flow at noon and at midnight caused by a large temperature difference between air and surrounding surfaces and, subsequently, less intense flow when the air was mixed up effectively. The temperature distribution in the cross-sections did not only indicate an increase in temperature with increasing height (up to 50 °C at noon) but also a temperature increase near the southern roof. The surface temperature of the masonry walls was stable (19–33 °C), while the air temperature fluctuated. The image of the flow was completed by ventilation through the tower, which acted as a solar chimney. The airflow through the door to the tower was almost 0.5 m^3 s^{-1} at summer midnight.

Keywords: thermodynamics; airflow network; CFD simulation; cultural heritage; wooden truss

Citation: Ponechal, R.; Krušinský, P.; Kysela, P.; Pisca, P. Simulations of Airflow in the Roof Space of a Gothic Sanctuary Using CFD Models. *Energies* **2021**, *14*, 3694. https://doi.org/10.3390/en14123694

Academic Editor: Ali Turan

Received: 23 February 2021
Accepted: 14 June 2021
Published: 21 June 2021

1. Introduction

The analysis of historic trusses, in addition to craftsmanship, geometry and stability, also examines the microclimate. Suitable climatic conditions in the attic space can have a positive effect on the service life of the structure. These conditions are mainly influenced by the attic ventilation and external weather conditions [1–5]. In addition to the wind and the temperature difference, the airflow during the attic ventilation is also affected by the solar radiation absorbed by the roofing, when the heated roofing increases the air circulation [6,7]. On the other hand, the heat storage capacity of the stone masonry structure of the walls and ceiling stabilizes the temperature [8,9]. In recent years Richter et al. have been dealing with the unheated attic spaces (so-called "cold attics") as one of the most moisture-problematic spaces in the building [10]. They stated that that the colder the climate is, the more advantageous the use of a ventilated attic becomes. In the most problematic regions, the design could be combined with a controlled ventilation system as suggested by study from Sweden [11]. According to the early Christian tradition, based on Didascalia Apostolorum from the early 3rd century, the apse in the medieval churches is oriented to the east [12]. In accordance with this ancient document, the temple is to point to the east oriented [13], which practically means that in most trusses, one main roof plane is always oriented to the south. While in the past the builders relied on empirical experience to a greater extent than at present, now they can also use computer simulation models to analyze how the construction behaves and how it works in principle [14–21]. When determining the airflow in large multi-story spaces, experiments with measurements on reduced models [22] are performed, simulations using validated models according to

full-scale measurements are also used [23]. They function effectively in the food industry when, for example, a fluid flow simulation analyzes the beverage production process in detail [24].

For the pilot application of the simulation approach described below in the research of possible airflow and temperature distribution in the attic space, a previously measured truss above the main nave of the Roman Catholic Church of the Corpus Christi in the historical center of the village Belá-Dulice was selected [25]. It is located in a rural environment at the foot of the Great Fatra in the district of Martin.

In a previous study [26], a multi-zone airflow network model (AFN) was used to simulate temperatures in the attic space in the building performance simulation (BPS) program, where space was divided into several closed zones. Then, in the calculation of AFN, the mass and energy conservation equations for each zone were solved to obtain a solution for the boundary conditions of the Ostrava city test reference year managed by International Weather for Energy Calculations (IWEC). The values are generated from a data bank longer than a year in duration, at least 12 years [27]. In this way, it is possible to simulate airflow quickly and relatively simply through the attic openings at any time and season. A detailed description of the airflow network model may be found in the work of Walton [28]. The disadvantage of the model is the use of unidirectional components that allow air to flow through the opening at a given time in only one direction. In practice, this means that it is not possible to model the rise of air in one part of the attic and its fall in the other part. The air in the whole attic simulation model at a given time either rises or falls. With this study, we wanted to verify whether and to what extent the simulation will agree with the measurement because the BPS program considers one average temperature for the whole zone. It does not consider the difference between the south and north-oriented half of the attic space. Likewise, the temperature varies stepwise along with the height of the zone.

These problems can be partially eliminated by using computer fluid dynamics simulation (CFD). It is a more computationally demanding simulation tool, so only a short period is usually simulated, not the whole year. Therefore, only the attic geometry, material characteristics of walls and roof, inlet and outlet openings for airflow are entered into the simulation model, while the air volume through these openings is adopted from the year-round BPS simulation with the AFN model. Particular strategies for coupling energy simulation and CFD programs are described in the paper by Zhai et al. [29]. A similar approach when coupling the simulation tools was used for whole heat and moisture transfer simulation was outlined by Koronthalyova [30] and for a double-skin façade assessment [31]. We started to examine the inner environment of attic spaces, which was preserved virtually intact for several centuries, by observing the most significant flow of air through the vents in the warm season.

In the triangular space of the truss, a natural flow is created on a sunny summer day caused by a large difference in the surface temperature of the first and the second roof or the stone masonry. The nature of the flow under these boundary conditions is well known from older experiments [32]. The question is how it will behave in a space with ventilation holes and how much these affect the nature of the flow on a windless day. Due to the efficient placement of a limited number of temperature, humidity and wood sensors, we identified places with high temperature and flow rate as well as places with low temperature and flow rate. These are potential areas for a causal analysis of the degradation of wooden truss elements.

2. Materials and Methods

The Roman Catholic Church is a single-nave building made of stone masonry, with a sanctuary with a straight end on the east side (Figure 1). It has a tower on the west side and a sacristy room on the north side of the sanctuary (Figure 2). It was built, like almost all medieval churches, in an east–west orientation, probably in the first half of the 14th century. In the 17th century, a tower was added to the church. In 1749, the nave of the

church was vaulted, until then the vault was only above the sanctuary and above the nave there was a wooden ceiling. The saddle roof has a roofing slope of 59°64′ with gable walls. The roof cladding consists of copper sheet roofing in strips [33].

Figure 1. South view of the Roman Catholic Church: tower, nave and sanctuary.

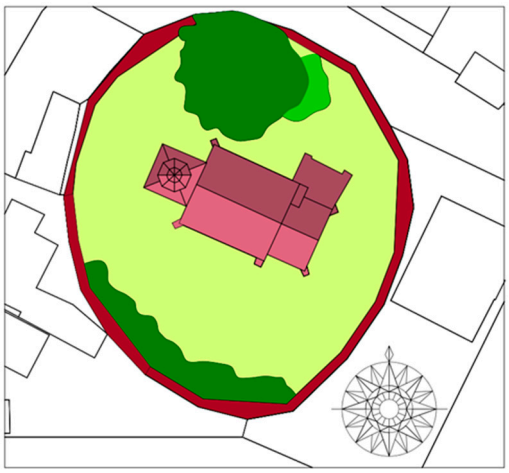

Figure 2. Top view as an illustration with the surrounding vegetation.

According to dendrological dating, the truss was built after 1409 from red spruce, making it one of the oldest medieval trusses in Slovakia. The construction is typical of medieval country churches with an optimally designed construction [34].

2.1. Examined Truss Roof Space

The truss is a rafter collar-beam construction with a longitudinal stiffening truss (Figure 3). It consists of ten (four full and two intermediate) ties. In the main roof truss, the collar beams cross the central king posts, which are lapped together with the rafters in the vertex. The posts are tenoned into a sill beam, longitudinally cogged on the connecting tie beams. Symmetrical braces stabilize the king post and connect it to the tie beam. The rafters are tenoned into the tie beams, while the transverse stability is ensured by high transverse struts. The joints here are dovetail overlaps. The tie beams are cogged on simple wall beams. In the longitudinal direction, the truss is braced by a longitudinal frame stool, which consists of a frame of a sill beam and four posts, separated by the horizontal struts at approximately half the height [35].

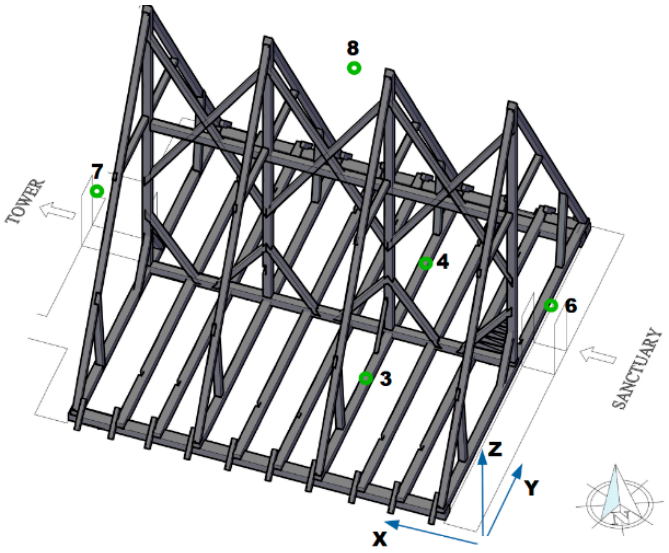

Figure 3. Side view of the truss over the nave with the location of the measuring points. The arrows indicate the openings to the tower and the truss above the sanctuary.

2.2. Measuring System

The measuring system consists of sensors connected to a central unit with a source. The individual sensors, monitoring the temperature and humidity of the environment, were located in key positions within the truss. In this way, based on the results of long-term measurements and subsequent simulations, an exact idea of the parameters of the truss's internal environment could be created. The primary parameters of interest were related to the humidity conditions important for understanding the location of places with a higher probability of biotic damage. The sensors were placed at 19 points, capturing the profile of the full tie, the second from the sanctuary, partly at the extreme ties at the gable walls [25]. The measurement results were published in previous articles, here we present only the basic values as the maximum and minimum recorded temperature on a hot summer day (Table 1). Out of the total number of 19 sensors, 5 are documented here, their position is marked in Figure 3.

Table 1. Selected measurement results of the air temperature in the truss according to the sensor position on 3 June 2012.

Sensor No.	X Direction (m)	Y Direction (m)	Z Direction (m)	Maximum of Daily Air Temperature (°C)	Minimum of Daily Air Temperature (°C)
3	3.8	2.5	0.3	27.7	15.5
4	3.8	5.9	0.3	27.4	10.7
6	0	4.4	1.5	25.0	14.9
7	9.4	4.7	1.5	25.4	15.4
8	4.7	4.2	8.4	47.7	14.4

2.3. Dynamic BPS Model

The BPS simulation calculation considering the accumulation of heat in the walls, floor and the mass of the wooden truss was performed in the EnergyPlus program from 12 separate zones (Table 2). The zones are connected by an AFN model of natural ventilation via appropriate unidirectional components determined by the equivalent opening area and the flow discharge coefficient. The lower zone represents the space of the church, the attic above the church in its height is divided into 5 zones, the attic above the sanctuary as well as the tower are divided into three zones (Figure 4).

Table 2. BPS zone model characteristics.

Zone	Volume (m^3)	Zone	Volume (m^3)	Zone	Volume (m^3)
Sanctuary_1	89.20	Nave_1	216.65	Tower_1	66.88
Sanctuary_2	45.38	Nave_2	105.78	Tower_2	84.80
Sanctuary_3	47.97	Nave_3	114.33	Tower_3	64.00
		Nave_4	30.78	Church	137.66
		Nave_5	9.29		

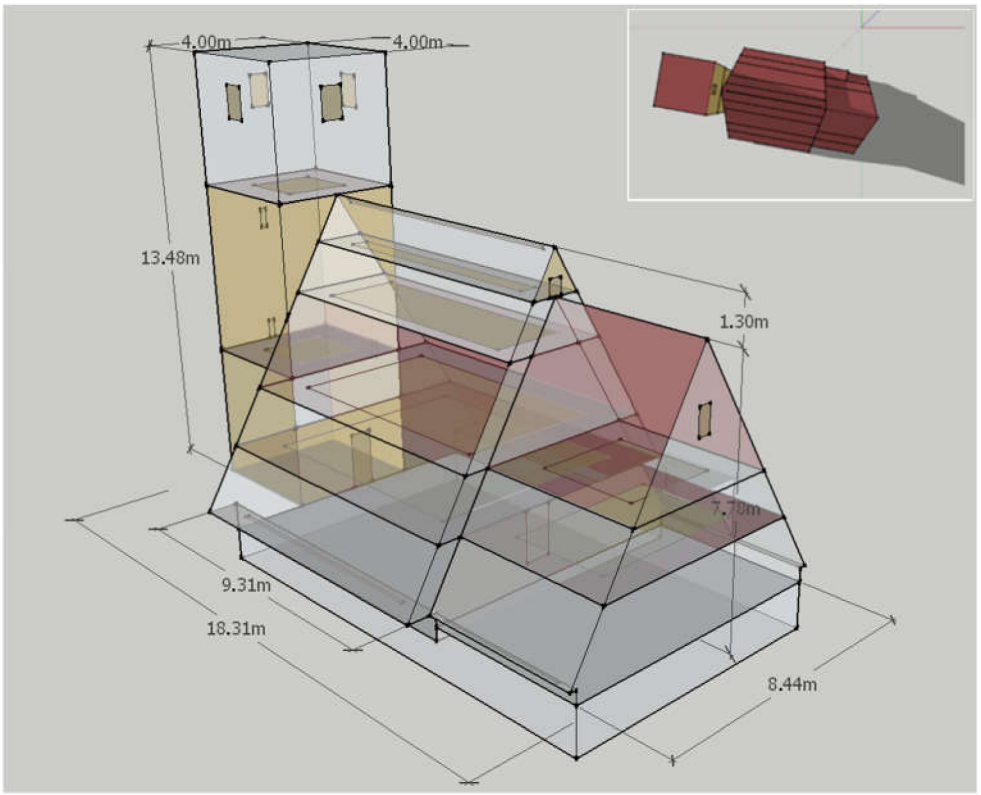

Figure 4. Side view of the BPS model with dimensions (a top view with the cast shadow on 6.6. at 6:00 p.m. in right-top corner).

From the results of temperature measurement with temperature sensors in May and June 2012, it is possible to identify an increase in temperature during sunny days. The temperature rises with the height of the sensor during the afternoon, while in the evening and at night the temperature in the attic equalizes. During cloudy days, the temperatures in the attic are balanced throughout the day. The simulation calculation copies the rise in air temperature based on height during a sunny day. There are minor differences in the absolute values compared with the measured values.

2.4. CFD Airflow Model

To consider the asymmetric airflow in the attic due to the heating of individual roof surfaces from solar radiation, a separate model was created in DesignBuilder CFD standalone module without linking to EnergyPlus [36]. The steady-state governing equations were solved using a SIMPLER (Semi-Implicit Pressure Linked Equations) algorithm, as a numerical procedure to solve incompressible Navier–Stokes equations. The SIMPLE algorithm uses an approach where the equations are solved in sequential steps letting to the iterative process. The equations comprise a set of coupled non-linear second-order

partial differential equations having the following general form [37], where δ represents any dependent variable (temperature, velocity, mass, turbulence and kinetic energy):

$$\frac{\partial}{\partial t}(\rho\delta) + div\,(\rho v\delta) = div(\tau\ grad\ \delta) + G \quad (1)$$

t denotes time (s), ρ density of air (kg m^{-3}), υ kinematic viscosity of air (kg m^{-1} s^{-1}), τ diffusion coefficient for δ and G is a source term. Turbulence was modeled using the k-ε model. The structured mesh was automatically generated by identifying all contained model objects edges with a hybrid discretization scheme. Mainly due to the representations of the sloping roof plane into the rectangular grid, smaller default grid spacing was used (Figure 5). The grid independence was tested by calculating air temperature in attic space (Figure 6). The air temperature in the selected cell stabilizes over 1 million cells. Therefore, each CFD simulation in this study was performed using 86 cells in the x-direction, 104 in the y-direction and 93 in the z-direction. On the other hand, for the sake of clarity, images generated from a calculation with a less dense network are presented. (It is not possible to reduce the number of vectors in the program). This is not an obstacle, as there are only minor differences in the flow and air temperature. The models converged after approximately 3000 iterations, when normalized residuals dropped to 10^{-5}.

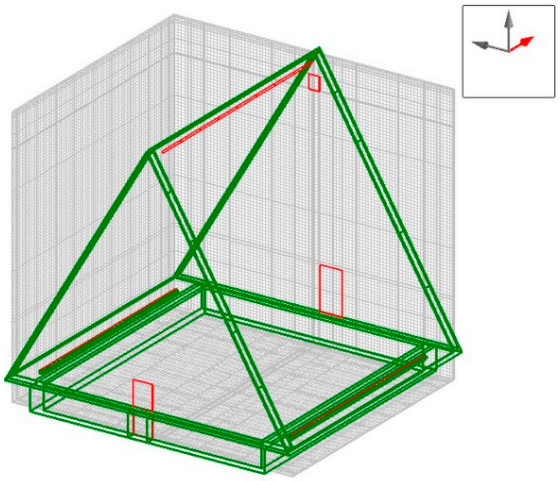

Figure 5. Three-dimensional CFD model and mesh structure with 0.8 million cells (openings are in red).

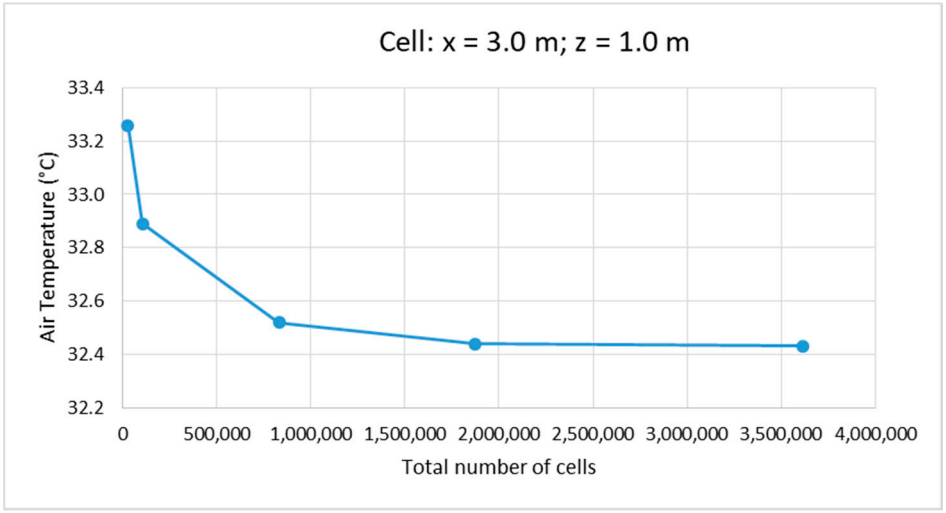

Figure 6. Sensitivity test of different network densities.

The CFD simulation was used as a stand-alone module. The boundary conditions such as surface temperatures and airflow through openings were established manually from previously calculated variables using the EnergyPlus software. The individual roof and wall surfaces were divided according to their size into the zones of the BPS model in the EnergyPlus simulation program. According to the simulation results in this program, fixed values of surface temperatures, flow rates and air temperature at the inlet to the stationary CFD model were entered.

3. Results

The most important factors that specify the nature of the flow are the surface temperature of the roof and the volume of air passing through the openings. These parameters were obtained by dynamic simulation (BPS) with the AFN model of natural ventilation through the unidirectional components in summertime. Based on this, one day with the highest simulated air temperature in the upper part of the attic (exactly at 12:00 p.m.), was selected (Figure 7). It was a sunny windless day. On this day, four states of the given environment were documented, corresponding to the simulated states from 6.6. at 12:00 and 18:00 and from the following night and morning on 7.6. at 2:00 and 6:00, which is a typical summer one-day cycle.

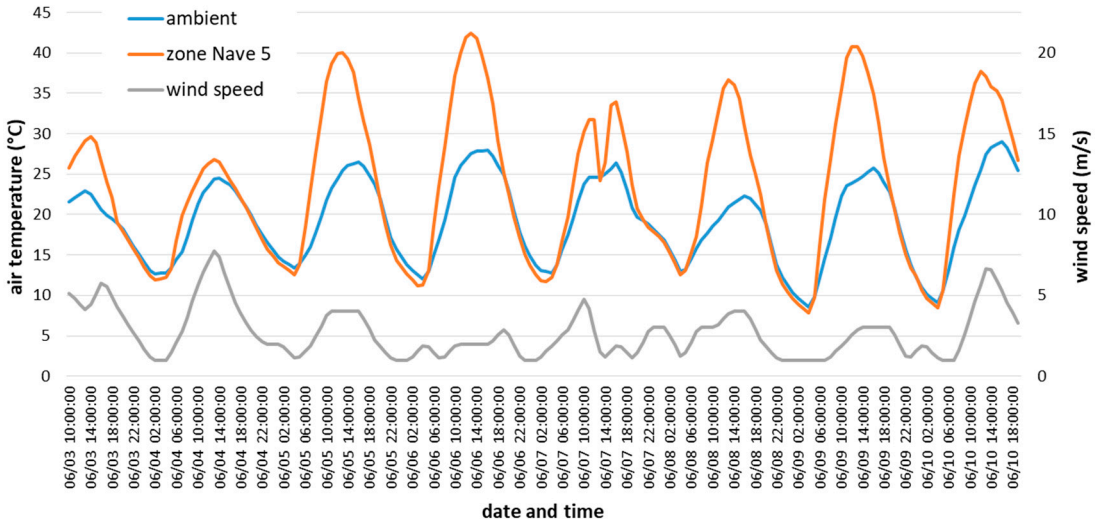

Figure 7. Simulated course of air temperature in the uppermost part of the attic space (zone Nave_5).

3.1. Airflow Simulation Results at Noon

The largest air movement in the attic occurs in the summer at noon. This is because one roof plane is oriented to the south and the other to the north. The dark-colored metal roofing heats up to a temperature above 60 °C on the south side (see Table 3). The heated air from the roofing starts to rise sharply and causes high air temperatures in the upper part of the attic space (higher than 50 °C). The heated air causes overpressure in the upper part, but the air cannot escape through the relatively small opening at the top. Instead, it changes direction in the motion, bypasses the cooler north roof and stone masonry walls (Table 4), and cools down. This creates a large air vortex, which in late the afternoon causes the homogenization of the air temperature in the entire attic space.

Table 3. Airflow characteristics through the openings at 12:00 a.m. obtained from BPS simulation.

Opening	Area (m^2)	Airflow ($m^2 \cdot s^{-1}$)	Velocity ($m \cdot s^{-1}$)	Air temperature (°C)
door to the tower	1.260	0.37	0.29	24
slots in the soffit—south side	0.731	0.04	0.05	27.5
slots in the soffit—north side	0.731	0.04	0.05	27.5

Table 4. Surface temperatures at 12:00 a.m. obtained from BPS simulation.

Surface	Temperature (°C)	Surface	Temperature (°C)
roof—north side	32–39	attic floor	23
roof—south side	57–61	stone masonry walls	23–33

At 12:00 a.m., there was the largest airflow through the upper opening out of the attic space also. Colder air (24 °C) was sucked in relatively massively from the space of the adjacent tower. Ventilation through the slot in the soffit was not highly intense at that time (Figure 8).

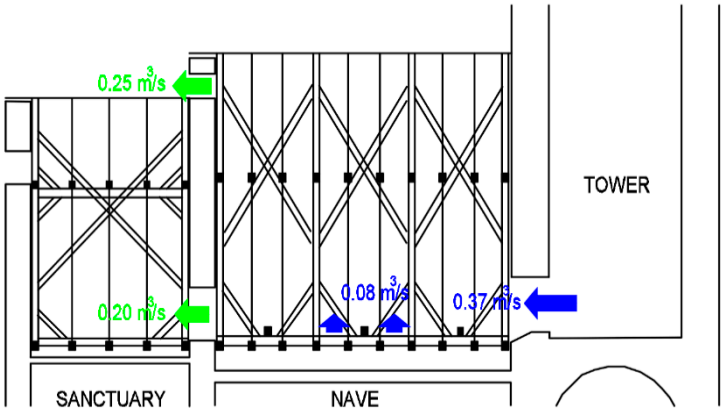

Figure 8. Airflow paths at 12:00 a.m. obtained from BPS simulation in section (blue—inlet, green—outlet).

The static CFD simulation considers the difference between the south and north-oriented half of the attic space and the stratification of the air temperature along the height of the zone. It displays a more accurate image of the airflow in the attic and how it is affected by the temperature of individual surfaces. The color scale of the texture determines the distribution of air temperatures in a given cross-section. The direction of airflow is given by a vector whose color determines the speed of airflow in the cross-section (Figure 9).

The nature of the airflow is not only influenced by the airflow through the ventilation openings but also by the increased airflow rate due to heating from the surface of the south roof. In the longitudinal section, we can see the falling and cooling of the air along the walls of the tower and the sanctuary. The airflow in the longitudinal section is also affected by the airflow through the inlet and outlet openings. The increased airflow rate due to the heating of the south roof manifests more in the middle with a speed of 0.25 to 0.33 m/s. In the case of walls, the flow rate is lower due to their cooling capacity. The flow rate is also increased at the inlet and outlet openings. Through the inlet opening from the tower, air flows at a speed of 0.29 m/s. By mixing with falling air next to the tower wall and air circulation caused by heating the south side of the roof its speed increases up to values of approximately 0.57 m/s. The speed also increases when the air is discharged through the ventilation opening above the sanctuary with the achieved values of 0.57 to 0.65 m/s. The air discharged through the door into the sanctuary reaches a lower flow rate of approximately 0.25 m/s, colder air descending along the wall and cooler air near the door is discharged.

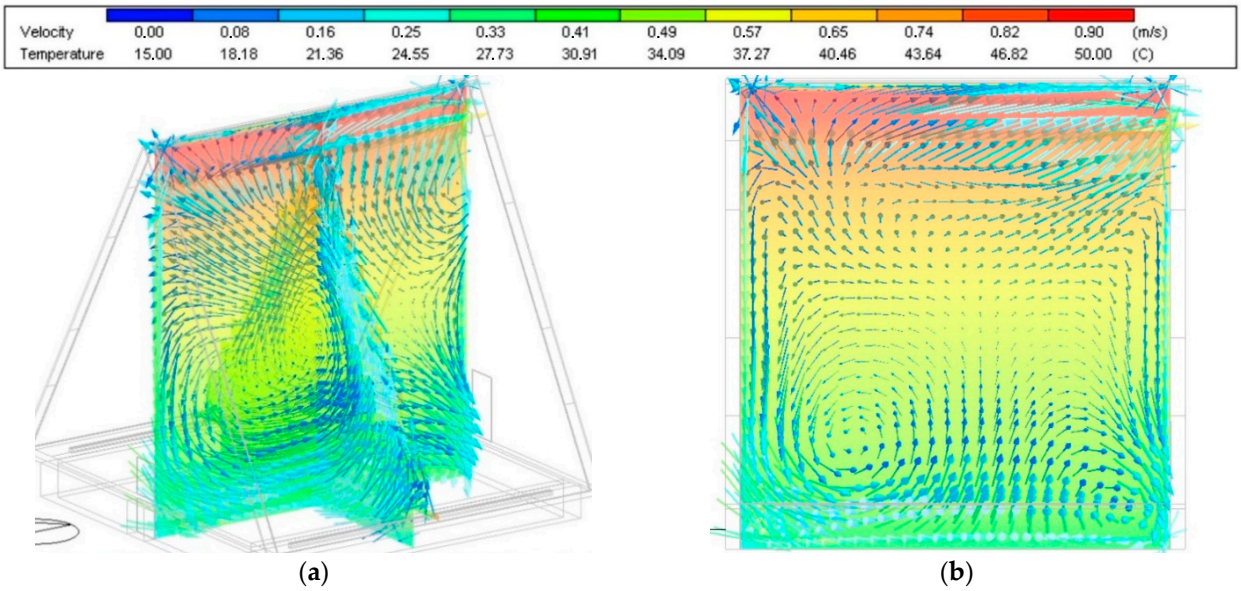

Figure 9. Simulated airflow paths on 6.6. at 12:00 a.m. in position of: (**a**) transverse sections; (**b**) longitudinal section.

In the cross-sections (Figure 10), we can notice the flow asymmetry at the extreme sections caused by the ventilation holes and cooling from the walls. In the middle, the air mixing is relatively symmetrical, but the airflow rate changes significantly. It is markedly higher along the surface of the southern roof, where it reaches a speed of 0.25 to 0.49 m/s. At the northern roof, there is an air decrease in air, which has a slower character of 0.08 to 0.25 m/s. The temperature distribution in the longitudinal section is similar to that shown in previous AFN simulations. The coldest air is at the ceiling with a temperature of 23 °C, (the proximity to the ceiling causes its cooling). By mixing with the supplied air from the tower and the air circulating in the attic, the air temperature near the ceiling is 24 to 27 °C.

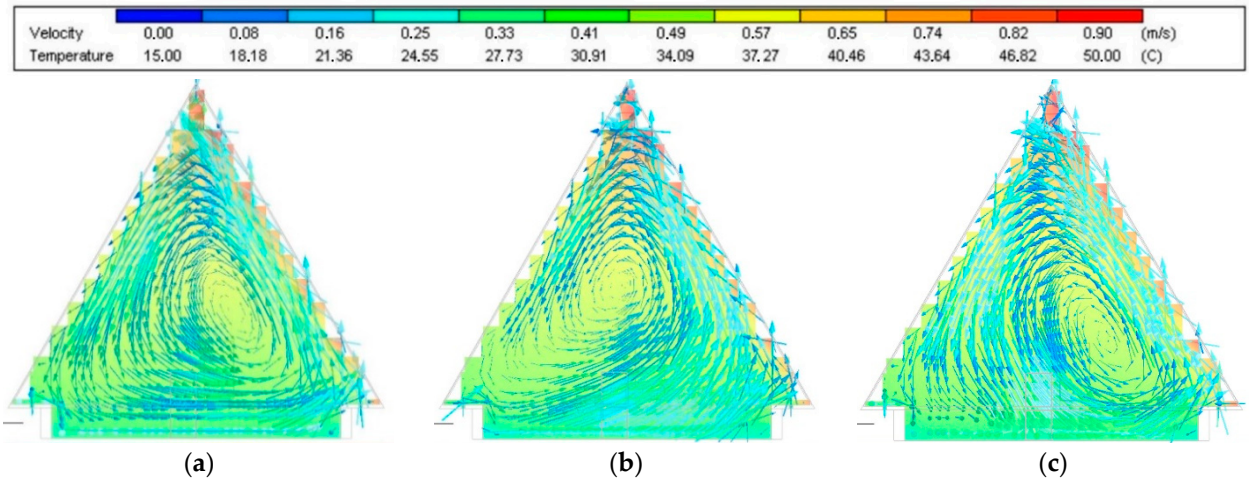

Figure 10. Simulated airflow paths on 6.6. at 12:00 a.m. in cross-section: (**a**) 0.8 m from the sanctuary wall; (**b**) in the middle of attic space; (**c**) 0.8 m from the wall of the tower.

The air temperature increases with height. At the top of the roof, it reaches temperatures above 50 °C. Slight cooling of the hot air is visible at the walls and at the ventilation opening above the sanctuary. The temperature distribution in the cross-sections provides us with a more satisfactory image of the airflow, as not only an increase in temperature with increasing height is visible but also an increase in temperature near the southern roof where temperatures reach 43 to 46 °C and above 50 °C in very close proximity to the roof. On the contrary, the temperatures at the northern roof reach values of 34 to 37 °C.

Based on the flow images from the CFD, it can be stated that in the middle of the space there is an area with predominantly low airflow velocities, while around the wall and roof surfaces the velocity increases. In these places, we can expect an increased effect of airflow on the change of wood moisture.

3.2. Airflow Simulation Results in the Evening

In the evening, the sun's rays fall on the roof at an acute angle. In addition, the roof is shaded by the west-facing tower. The temperature of the thin metal roofing drops rapidly, which has a significant impact on the airflow character in the attic—it changed completely. The air temperature in the attic will be unified and the air will flow slowly in the opposite direction, i.e., downwards from the upper opening (Figure 11). The slight overpressure in the simulation model caused by the flow of air into the attic through the upper opening, the door from the tower and from the adjacent truss is compensated by the discharge through the slot in the soffit at the wall beam (Figure 12).

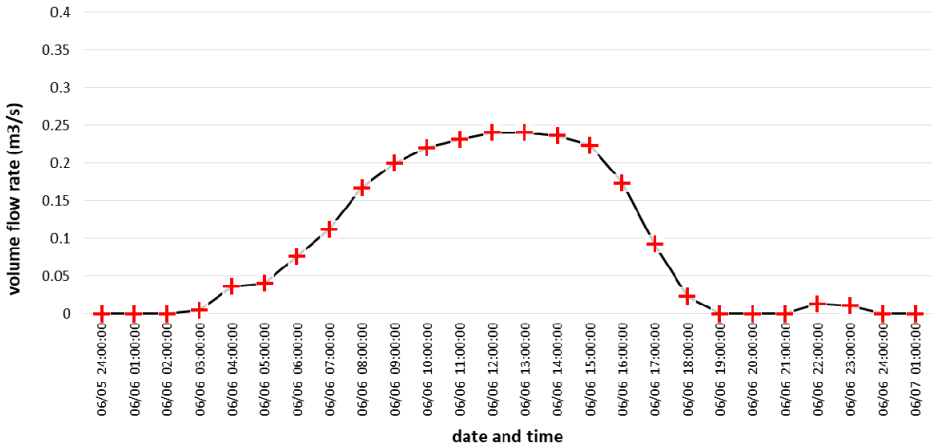

Figure 11. Simulated course of volume flow rate through the upper opening from the attic to the outside.

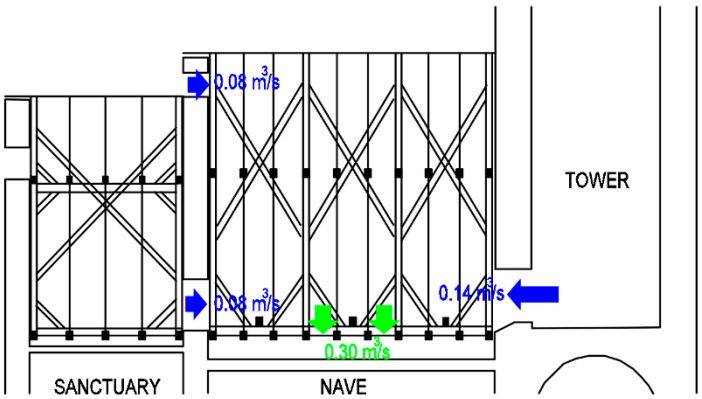

Figure 12. Airflow paths at 6:00 p.m. obtained from BPS simulation in section (blue—inlet, green—outlet).

The flow through the upper window out of the model slowed down until it ended at 6:00 p.m. At this time, the air in the simulation model flows into the truss space also through the tower door and through an opening from the adjacent truss. The attic space is slightly cooled by the air (22 °C) coming from the tower (Table 5). Most of the roof is shaded at this time and the roofing is no longer hot, its temperature is only 23–25 °C (Table 6). There is no longer a significant difference in the temperature of the roofing on the south and north side.

Table 5. Airflow characteristics through the openings at 6:00 p.m. obtained from BPS simulation.

Opening	Area (m^2)	Airflow ($m^3 \cdot s^{-1}$)	Velocity ($m \cdot s^{-1}$)	Air Temperature (°C)
door to the tower	1.260	0.14	0.11	22
door to the next loft	1.232	0.08	0.06	24
upper opening	0.200	0.08	0.40	25

Table 6. Surface temperatures at 6:00 p.m. obtained from BPS simulation.

Surface	Temperature (°C)	Surface	Temperature (°C)
roof—north side	24	attic floor	23
roof—south side	23–25	stone masonry walls	23–27

The nature of the airflow is influenced mainly by the flow of cold air through the door from the tower and cooling from the ceiling above the church, which can be seen in the longitudinal section (Figure 13). Unlike the previous state, we can notice that in the close vicinity of the walls there is no falling and cooling of the air, but on the contrary, its rise and slight heating occurs. The surface of the walls is now at a higher temperature than the supplied air. In the longitudinal section, it is visible as the cold air supplied from the tower passes along the ceiling surface at a relatively low velocity of 0.04 to 0.1 m/s and rises in the second half of the space due to the air supplied from the sanctuary door. Here, the flow velocity from the warmer wall increases to values of 0.21 to 0.24 m/s. The warmest air flows at the top of the roof due to the supply of warm air through the ventilation opening and is mixed with the airflow along the wall. This increases the temperature and the speed of the airflow towards the tower with the flow speed of 0.34 to 0.38 m/s at the top of the roof. The air then falls near the wall of the tower. In close proximity to the tower wall, the heated airflow rises at lower speeds, and at the top of the roof, it is mixed with the air flowing from the sanctuary wall and then decreases near the tower wall. The position of the falling air is caused mainly by the velocities of the airflow and its mixing. In cross-sections (Figure 14), the flow is relatively symmetrical as the surface temperatures of the south and north walls are approximately identical. Ventilation slots in the soffit, through which cooler air passes, significantly contribute to the air movement and thus cause a decrease in cooler air in the space. This decrease is visible in the central section and the section near the tower wall. In the section near the wall of the sanctuary, the rise and heating of the air and the increasing flow velocity along the height of the wall from 0.08 up to 0.33 m/s are visible. The temperature distribution in the longitudinal section indicates the highest temperatures at the top of the roof of approximately 24 °C.

Significant air heating is visible from the walls with increasing height. The temperature at the walls at the top of the roof is approximately 25 °C. The heated air is directed into space where it is mixed with the cooler air and then falls, due to the ventilation slots and the flow of cold air supplied through the opening from the tower. The temperature distribution in the cross-sections is symmetrical with increasing temperature along the truss height with a temperature of 23 °C at the ceiling above the nave, 24 °C at the top of the roof in the middle and 25 °C at the top of the roof at the walls.

The overall character of the airflow is thus most influenced by the air supplied from the tower, cooling from the ceiling and heating from the wall surfaces. The movement of air at the top of the roof is also affected by the ventilation opening above the sanctuary, but the predominant influence is the rise of air along the wall height.

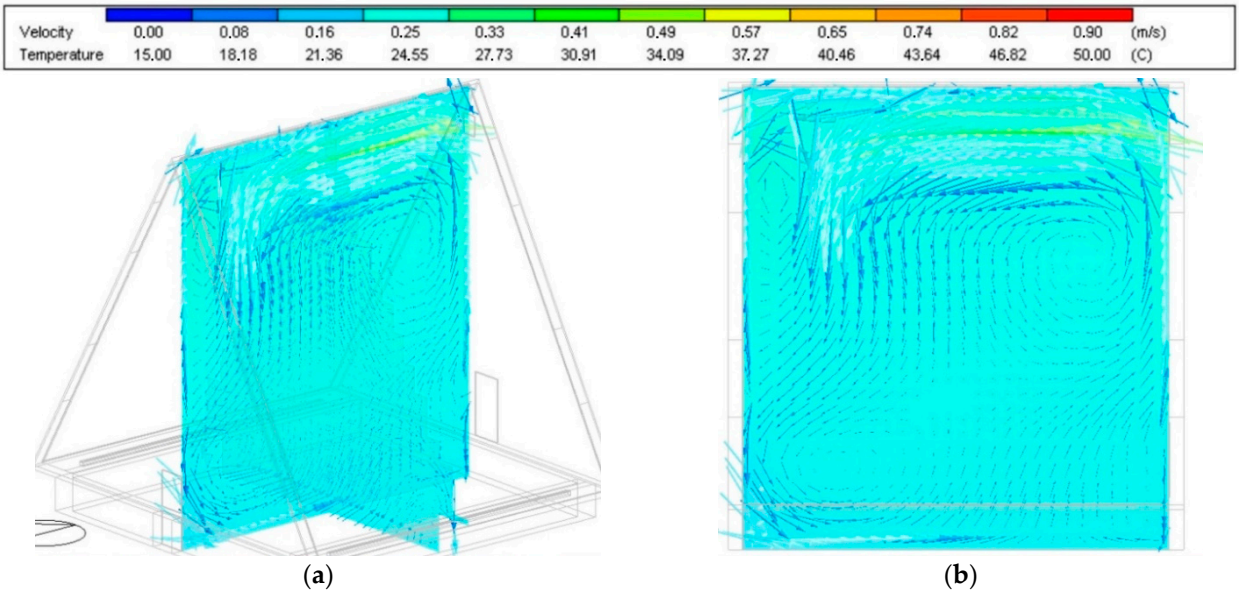

Figure 13. Simulated airflow paths on 6.6. at 6:00 p.m. in position of: (**a**) transverse sections; (**b**) longitudinal section.

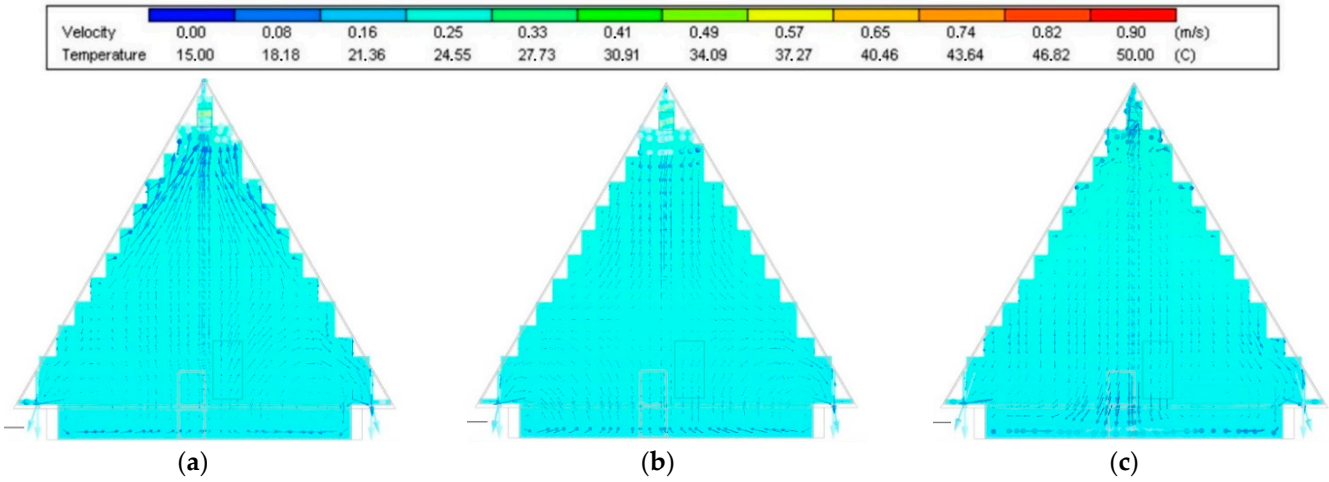

Figure 14. Simulated airflow paths on 6.6. at 6:00 p.m. in cross section: (**a**) 0.8 m from the sanctuary wall; (**b**) in the middle of attic space; (**c**) 0.8 m from the wall of the tower.

3.3. Airflow Simulation Results at Midnight

At night, there is an occurrence of the tower effect, which fulfills the function of the so-called solar chimney [38] or wind tower as a device that allowed the effective use of natural ventilation in the hot Middle East regions for many centuries [39]. Hughes et al. summarized several studies related to the UK climatic conditions. They presented a review showing that wind tower ventilation has its justification based on regional characteristics and thermal conditions [40]. Between 0:00 and 2:00 at night, the airflow from the attic to the tower was strongest (Figure 15). At this time, in the simulation, the air is fed into the attic space through the door to the adjacent truss (slightly heated with a temperature of 16 °C) and through the slots in the soffit (cold exterior with a temperature of 13 °C) (Table 7). The upper vent is now ineffective. The cold air in the tower heats up from the heated stone masonry walls and rises upwards (Figure 16). This creates a negative pressure in the truss space, which, according to the result of the simulation calculation, is compensated by supplying cold exterior air through the slot in the soffit at the wall beam. A similar effect as in the tower occurs in the attic space, where the air heated by the warmer stone gable walls rises and then cools down in the center of the attic space. This is a flow typical of

atriums—open spaces over several floors [41]. An important role here is played by the accumulation capacity of historic stone masonry, which heats up only slightly during the day and only slightly cools down at night. Such a temperature at night is a result of the low outside air temperature (13 °C) as well as the low surface temperature of the sheet metal roofing (10–12 °C). Such a low temperature of outdoor air at night is not common in Slovak climatic conditions and results from the location of the studied object in the foothills (on the edge of the Great Fatra National Park at an altitude of 512 m above sea level). The roofing has a very low temperature (see Table 8) (2 °C lower than the air temperature).

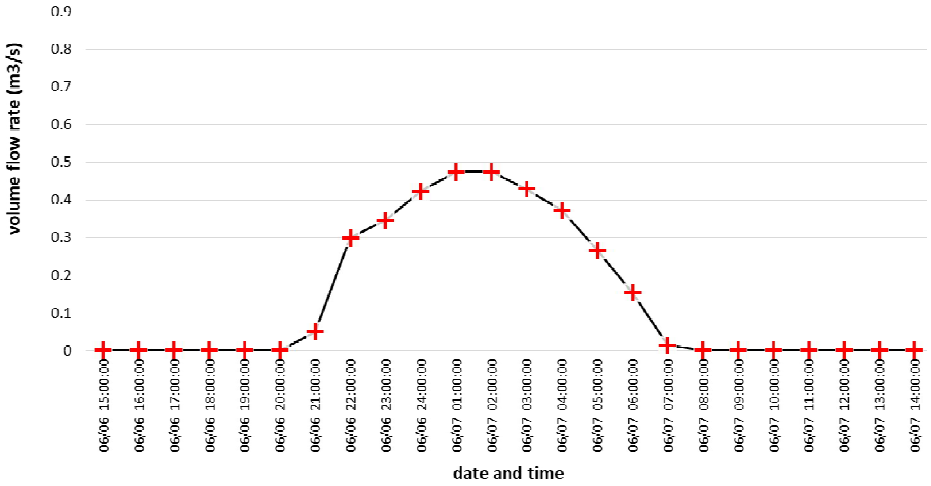

Figure 15. Simulated course of the volume flow rate through the opening towards the tower.

Table 7. Airflow characteristics through the openings at 2:00 a.m. obtained from BPS simulation.

Opening	Area (m^2)	Airflow ($m^2 \cdot s^{-1}$)	Velocity ($m \cdot s^{-1}$)	Air Temperature (°C)
door to the next loft	1.232	0.12	0.10	16
slots in the soffit—south side	0.731	0.15	0.21	13
slots in the soffit—north side	0.731	0.15	0.21	13

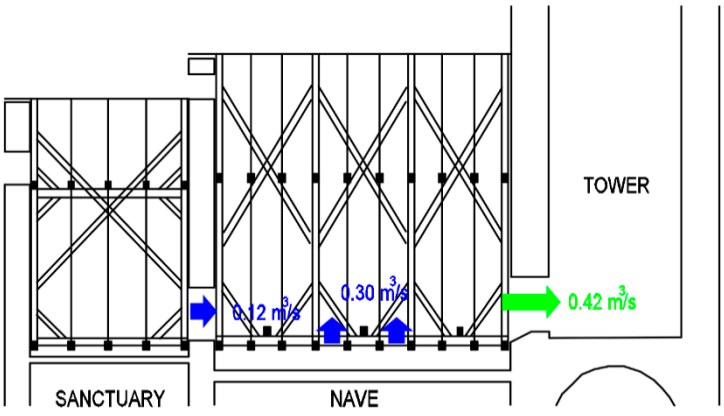

Figure 16. Airflow paths at 2:00 a.m. obtained from BPS simulation.

Table 8. Surface temperatures at 2:00 a.m. obtained from BPS simulation.

Surface	Temperature (°C)	Surface	Temperature (°C)
roof—north side	10–12	attic floor	20
roof—south side	10–12	stone masonry walls	19–20

The nature of the airflow is influenced by the supply of cold air through the ventilation slots in the soffit and from the door of the sanctuary. Its movement is directed by the heating from the walls. In the longitudinal section (Figure 17), there is visible air circulation caused by the heating of the air from the walls of the tower and the sanctuary. The air drawn in through the ventilation slots is redistributed and directed towards the walls. Most of the air is led towards the sanctuary wall because here the air is also sucked in through the sanctuary door and the speed of the airflow and thus the air circulation is greater here than at the tower wall. This creates two airflows along the walls leading to the top of the roof, where they mix and subsequently decrease in the direction of the circulation flow. The airflow velocities are highest at walls where they reach values of 0.47 to 0.54 m/s and by airflow mixing. The lowest speeds are in the middle of circulations, or in the middle of air vortices. In cross-sections (Figure 18), the flow is relatively symmetrical at the wall of the sanctuary, where the suction of air through the ventilation slots in the soffit and its rise and heating near the surface of the wall of the sanctuary is clearly visible. In the middle section, the air falling is visible when the flows of the two circulations are mixed. In a given section, the flow is faster at the top of the truss than in a flow of falling air, because the mixing of the circulating air is closer to the wall of the tower. In the given section, we can observe a slower airflow circulating near the sanctuary wall. In the section at the wall of the tower, a slightly asymmetrical flow, caused by the suction of air through the door into the tower, occurs. The temperature distribution in the longitudinal section is mainly influenced by air circulation. The highest temperatures are close to the walls—approximately 16 to 17 °C and the lowest temperatures in the middle of the circulating air—approximately 14 °C.

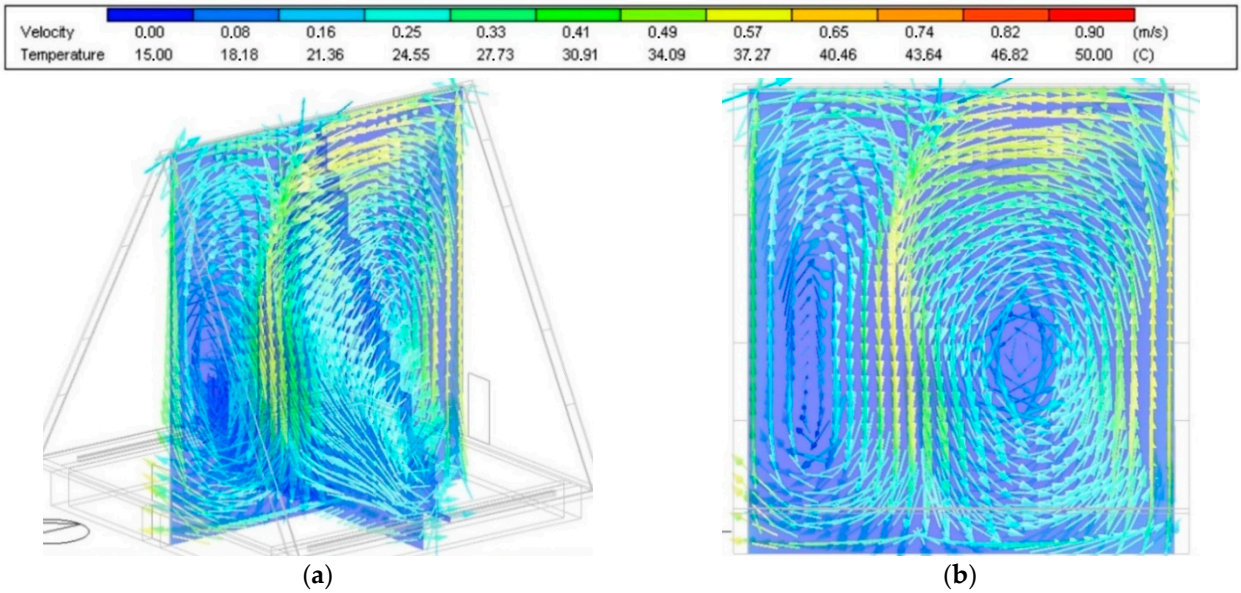

(**a**) (**b**)

Figure 17. Simulated airflow paths on 6.6. at 2:00 a.m. in position of: (**a**) transverse sections; (**b**) longitudinal section.

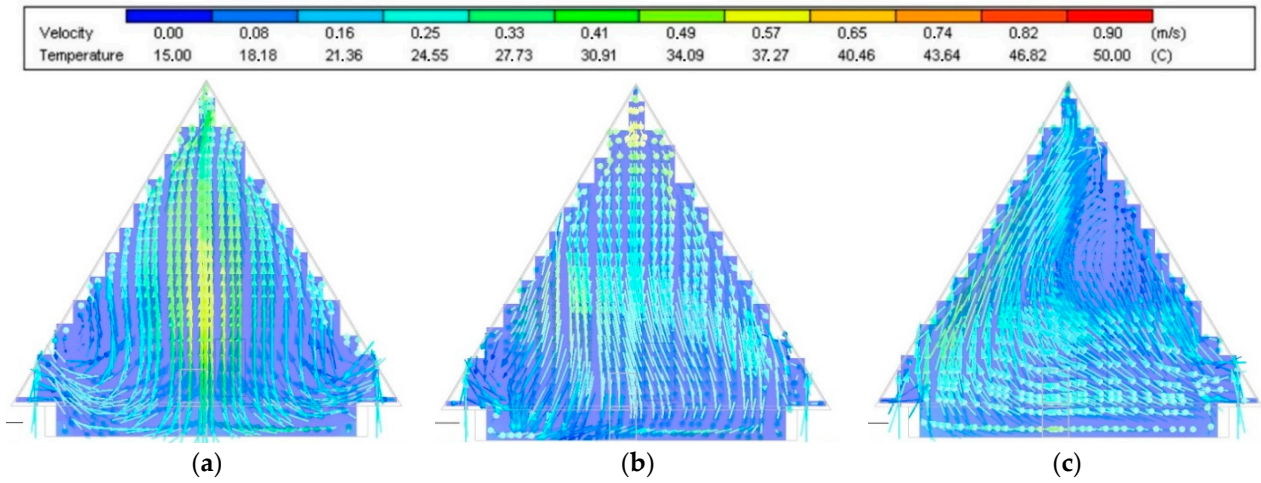

Figure 18. Simulated airflow paths on 6.6. at 2:00 a.m. in cross section: (**a**) 0.8 m from the sanctuary wall; (**b**) in the middle of attic space; (**c**) 0.8 m from the wall of the tower.

In cross-sections, the temperature distribution is influenced mainly by a slight cooling from the roof surface, where the temperature in close proximity is approximately 12 °C. Colder air is also present in the vicinity of the ventilation slots in the soffit. The air temperature rises towards the center at the extreme sections, which is caused by heating the air from the walls. The temperature difference is smaller at the middle section because the mixing of the two flows of circulating air occurs here. The overall character of the airflow is thus influenced mainly by the heating of the air from the walls of the tower and the sanctuary, which causes the circulation of the supplied air in two opposing flows.

3.4. Airflow Simulation Results in the Morning

In the early morning hours, the flow of air through the tower (the solar chimney) stops and a new equilibrium state occurs with a high-temperature homogeneity of the attic space. From this equilibrium state, the flow gradually changes to the typical morning when airflows from the tower and exits through an opening in the upper part of the truss (Figures 19 and 20). With sunshine and an increase in outdoor air temperature, in the morning of 7.6. the nature of the flow changes again and is similar to 6.6. at 12:00. Colder air (18 °C) begins to flow into the attic from the tower (Table 9) and through the slots in the soffit and exits through the upper ventilation opening. The air and the roof surface heat up slightly, with the air temperature and the surface temperature of the walls being approximately the same (Table 10).

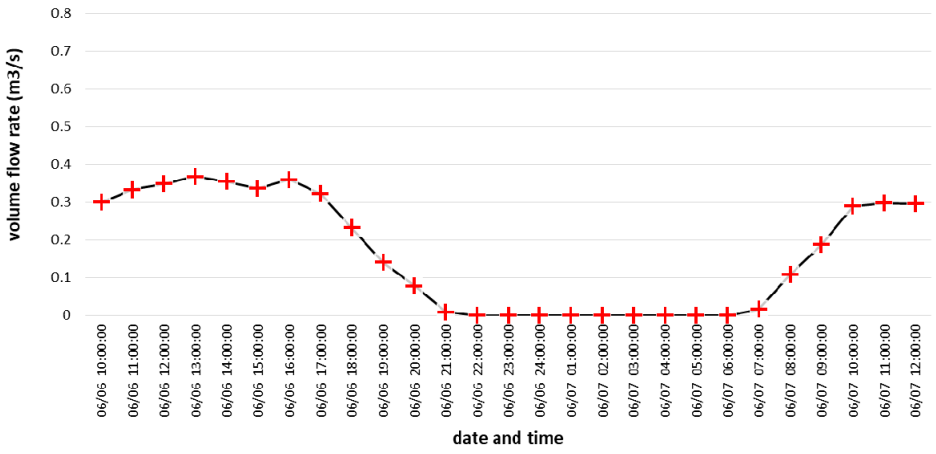

Figure 19. Simulated course of the volume flow rate through the tower into the attic.

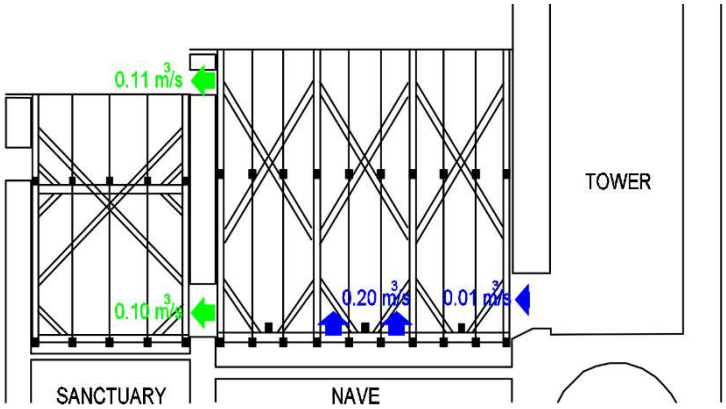

Figure 20. Airflow paths at 6:00 a.m. obtained from BPS simulation in section.

Table 9. Airflow characteristics through the openings at 6:00 a.m. obtained from BPS simulation.

Opening	Area (m^2)	Airflow ($m^2 \cdot s^{-1}$)	Mean Velocity ($m \cdot s^{-1}$)	Air Temperature (°C)
door to the tower	1.260	0.01	0.01	18
slots in the soffit—south side	0.731	0.10	0.14	17
slots in the soffit—north side	0.731	0.10	0.14	17

Table 10. Surface temperatures at 6:00 a.m. obtained from BPS simulation.

Surface	Temperature (°C)	Surface	Temperature (°C)
roof—north side	21–22	attic floor	20
roof—south side	21	stone masonry walls	19–21

In this case, the nature of the airflow is mainly influenced by the airflow through the ventilation openings because the surfaces of the walls and roof and the overall temperature distribution in the room are approximately identical. In the longitudinal section (Figure 21), the flow of air through the door of the tower is particularly visible. It is divided into a part of the air which is discharged through the door of the sanctuary and the ventilation opening and a part that circulates in the space. A slight air falling at the wall of the tower is influenced by a slightly lower wall temperature, but also because, unlike the wall of the sanctuary, there is no ventilation opening at the top which would, as with sanctuary the wall, direct the airflow. The air thus drops and circulates at the tower wall. The airflow speed is low at 0.05 m/s in the whole space. The slightly increased flow velocity of 0.13 m/s is 0.17 to 0.3 m/s at the tower wall and especially at the ventilation openings.

In cross-sections (Figure 22), air circulation, which has a relatively symmetrical shape, is visible. The direction of the circulating airflow is determined by a slightly higher temperature at the bottom of the north roof. The flow velocity is slightly increased at the surface of the northern roof—approximately 0.13 m/s, in the remaining space there are only small flow velocities at the level of about 0.05 m/s. There is lower air circulation in the section at the wall of the sanctuary because the heated air is exhausted through the ventilation opening above the sanctuary and the cooler air through the door to the sanctuary. In the middle, the air circulation increases, which is also contributed by the ventilation slots in the soffit. The air from the slot under the north roof flows mainly along the surface of the north roof, unlike the airflow from the southern slot, which flows near the ceiling. In the section at the tower wall, the circulating flow is shifted more towards the

warmer north roof and the flow of cooler air falls along the wall, where it mixes with the airflow coming through the tower door. The temperature distribution in the whole space is approximately identical—20 to 21 °C, a slightly increased temperature of 21 to 22 °C occurs at the roof surfaces and at the top of the truss. The lower air temperature of 19 to 20 °C is only in close proximity to the tower wall. The nature of the airflow here is influenced mainly by the flow of air supplied through the tower door and the air circulation, the direction of which is influenced by the temperature of the roof surface.

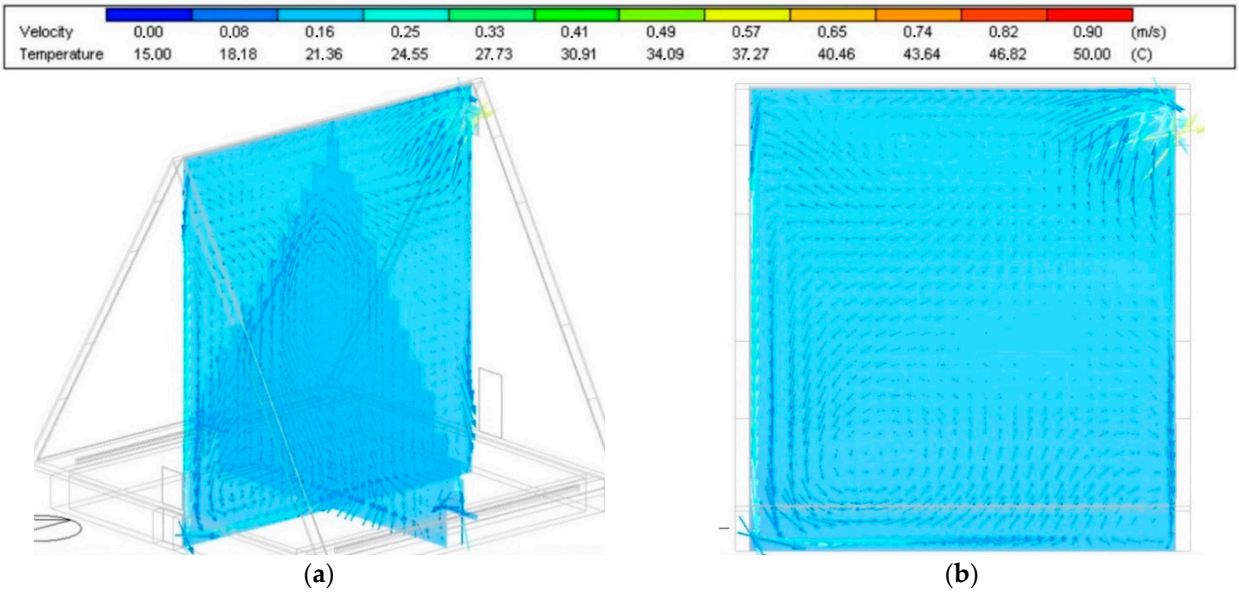

Figure 21. Simulated airflow paths on 6.6. at 6:00 a.m. in position of: (**a**) transverse sections; (**b**) longitudinal section.

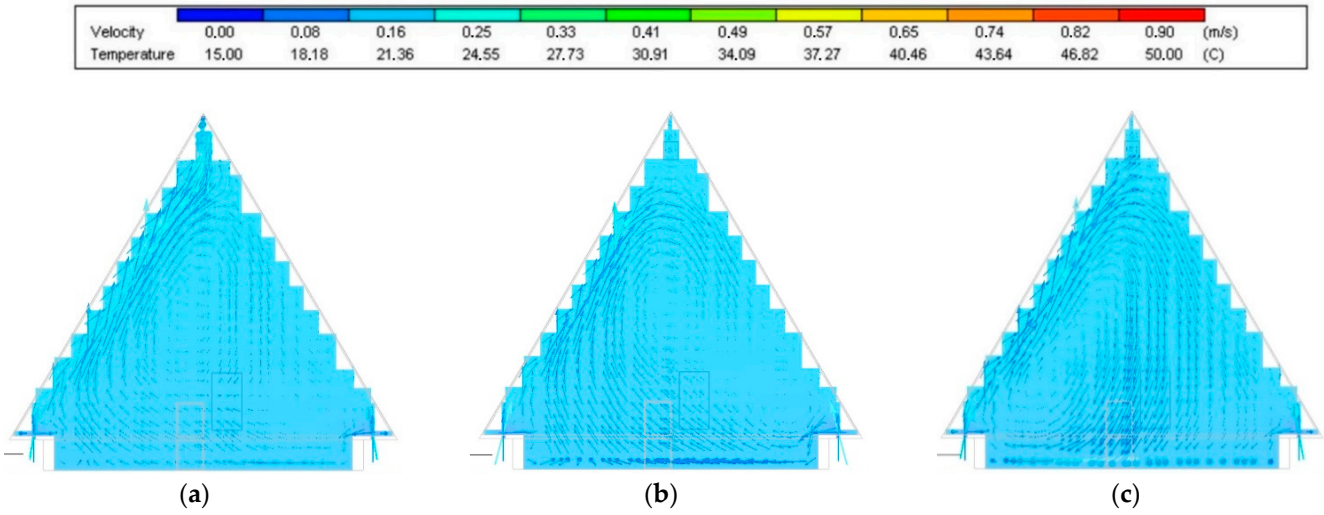

Figure 22. Simulated airflow paths on 6.6. at 6:00 a.m. in cross section: (**a**) 0.8 m from the sanctuary wall; (**b**) in the middle of attic space; (**c**) 0.8 m from the wall of the tower.

4. Conclusions

Using BPS simulation and AFN model of airflow, it was possible to simulate the rise and fall of air temperature in the truss during a hot summer day with sufficient accuracy. Using the zone dynamic model, we also accurately simulated the temperature distribution according to the height of the place. Though the agreement between the measurement and simulation was not as pronounced as in other studies [21,42].

During a typical summer day, when the sun's rays intensively heat the roofing in the morning, four characteristic states of air movement were documented using the CFD stationary simulation, adopting boundary conditions from BPS. These states changed at approximately 6-h intervals as in the analysis of coupled building energy and CFD simulations, where they also identified airflow and temperature patterns at four different moments in the middle plane of the test room without heating [29]. Two states feature more intense flow, which occurs at noon and at night and is caused by a large difference between air temperature and surface temperature. After these states, there are the states with the less intense flow, when the air is so mixed that the environment in the attic stabilizes in temperature.

Different as well as identical temperature conditions in the southern and northern part of the space during the day were simulated. The images from the CFD simulation demonstrated an increased airflow not only around the ventilation openings but also on hot (roof) and cold (gable wall) surfaces, where sensors for monitoring wood moisture will be placed in the future. The sensors will also need to be installed in the central part with minor air movement. The results can be transferred to almost all historical trusses in the respective region, as they are very similar [31] and identically oriented in terms of the cardinal directions. In the next step, we would like to focus on refining the airflow modeling by being able to calculate a dynamic model created directly in DesignBuilder simulation software. The program adopts the boundary conditions for CFD simulation automatically. It would also be advisable to verify the influence of the internal wooden elements of the truss, which create resistance to the flow of air and have not yet been considered.

We assume that this validated model provides a good starting point for examining the impact of different ventilation scenarios on the temperature and humidity in the truss. It will resemble the research in the interiors of historic buildings [15,16]. This research as well as our work confirm that CFD with a finite element modeling approach can provide basic support to the issues involved in the analysis and preventive conservation of ancient ventilation techniques in old buildings.

Author Contributions: Conceptualization, R.P. and P.K. (Peter Krušinský); methodology, R.P.; software, P.K. (Peter Kysela); validation, R.P., P.K. (Peter Kysela) and P.K. (Peter Krušinský); data curation, R.P., P.P.; writing—original draft preparation, R.P.; writing—review and editing, P.K. (Peter Kysela); supervision, R.P.; project administration, P.K. (Peter Krušinský); funding acquisition, P.K. (Peter Krušinský) All authors have read and agreed to the published version of the manuscript.

Funding: This research was funded by VEGA, grant number 1/0537/18.

Conflicts of Interest: The authors declare no conflict of interest.

Simulation Software: EnergyPlus 8.6.0; https://energyplus.net/ (accessed on 15 May 2021); Design Builder; Engineering Pro, V6; https://designbuilder.co.uk/ (accessed on 15 May 2021).

References

1. Walker, I.S.; Forest, T.W. Field measurement of ventilation rates in attics. *Build. Environ.* **1995**, *30*, 333–347. [CrossRef]
2. Kain, G.; Idam, F.; Federspiel, F.; Réh, R.; Krišťák, Ľ. Suitability of wooden shingles for ventilated roofs: An evaluation of ventilation efficiency. *Appl. Sci.* **2020**, *10*, 6499. [CrossRef]
3. Gullbrekken, L.; Kvande, T.; Jelle, B.; Time, B. Norwegian pitched roof defects. *Buildings* **2016**, *6*, 24. [CrossRef]
4. Nik, V.M.; Kalagasidis, A.S.; Kjellström, E. Assessment of hygrothermal performance and mould growth risk in ventilated attics in respect to possible climate changes in Sweden. *Build. Environ.* **2012**, *55*, 96–109. [CrossRef]
5. Hnilica, O.; Bichlmair, S.; Plášek, J. Indoor Climate in Jesuit Church of Holy Name of Jesus in Telc. In Proceedings of the CLIMA 2019, E3S Web of Conferences, Bucharest, Romania, 26–29 May 2019; Volume 111, p. 03056.
6. Wang, S.; Shen, Z.; Gu, L. The Impact of roof pitch and ceiling insulation on cooling load of naturally-ventilated attics. *Energies* **2012**, *5*, 2178–2196. [CrossRef]
7. Tariku, F.; Iffa, E. Temperature and air flow patterns in attic roofs. *J. Archit. Eng.* **2017**, *23*, 04017014. [CrossRef]
8. Tsilingiris, P.T. Thermal flywheel effects on the time varying conduction heat transfer through structural walls. *Energy Build.* **2003**, *35*, 1037–1047. [CrossRef]
9. Ponechal, R.; Staffenova, D. Insulation thickness versus dynamic thermal parameters of external walls with regard to the thermal stability. *Commun. Sci. Lett. Univ. Zilina* **2017**, *19*, 102–108.

10. Richter, J.; Staněk, K.; Tywoniak, J.; Kopecký, P. Moisture-safe cold attics in humid climates of Europe and North America. *Energies* **2020**, *13*, 3856. [CrossRef]
11. Hagentoft, C.-E.; Sasic Kalagasidis, A. Drying potential of cold attic using natural and controlled ventilation in different Swedish climates. *Procedia Eng.* **2016**, *146*, 2–7. [CrossRef]
12. Sparavigna, A.C. The solar orientation of the gothic cathedrals of France. *Int. J. Sci.* **2014**, *3*, 6. [CrossRef]
13. Gibson, M.D. *The Didascalia Apostolorum in English*; C.J. Clay: London, UK, 1903.
14. Lerma, C.; Borràs, J.G.; Mas, Á.; Torner, M.E.; Vercher, J.; Gil, E. Evaluation of hygrothermal behaviour in heritage buildings through sensors, CFD modelling and IRT. *Sensors* **2021**, *21*, 566. [CrossRef]
15. Bartak, M.; Drkal, F.; Hensen, J.L.M.; Lain, M.; Matuska, J.; Schwarzer, J.; Sourek, B. Simulation to Support Sustainable HVAC Design for Two Historical Buildings in Prague. In Proceedings of the 18th Conference on Passive and Low Energy Achitecture, PLEA, Florianópolis, Brazil, 7–9 November 2001; pp. 903–908.
16. Balocco, C.; Grazzini, G. Numerical simulation of ancient natural ventilation systems of historical buildings. A case study in Palermo. *J. Cult. Herit.* **2009**, *10*, 313–318. [CrossRef]
17. D'Agostino, D.; Congedo, P.M. CFD modeling and moisture dynamics implications of ventilation scenarios in historical buildings. *Build. Environ.* **2014**, *79*, 181–193. [CrossRef]
18. Balocco, C.; Petrone, G.; Cammarata, G. Numerical multi-physical approach for the assessment of coupled heat and moisture transfer combined with people movements in historical buildings. *Build. Simul.* **2014**, *7*, 289–303. [CrossRef]
19. Wang, S.; Shen, Z.; Gu, L. Numerical simulation of buoyancy-driven turbulent ventilation in attic space under winter conditions. *Energy Build.* **2012**, *47*, 360–368. [CrossRef]
20. Oetelaar, T. CFD, Thermal Environments, and Cultural Heritage. Two Case Studies of Roman Baths. In Proceedings of the 16th International Conference on Environment and Electrical Engineering (EEEIC) (IEEE, 2016), Florence, Italy, 7–10 June 2016; pp. 1–6.
21. Grau-Bové, J.; Mazzei, L.; Strlic, M.; Cassar, M. Fluid simulations in heritage science. *Herit. Sci.* **2019**, *7*, 12. [CrossRef]
22. Lu, Y.; Dong, J.; Wang, Z.; Wang, Y.; Wu, Q.; Wang, L.; Liu, J. Evaluation of stack ventilation in a large space using zonal simulation and a reduced-scale model experiment with particle image velocimetry. *J. Build. Eng.* **2021**, *34*, 101958. [CrossRef]
23. Albuquerque, D.P.; Mateus, N.; Avantaggiato, M.; da Graça, G.C. Full-scale measurement and validated simulation of cooling load reduction due to nighttime natural ventilation of a large atrium. *Energy Build.* **2020**, *224*, 110233. [CrossRef]
24. Stachnik, M.; Jakubowski, M. Multiphase model of flow and separation phases in a whirlpool: Advanced simulation and phenomena visualization approach. *J. Food Eng.* **2020**, *274*, 109846. [CrossRef]
25. Korenkova, R.; Krusinsky, P.; Pisca, P. Analysis of the impact of microclimate in a roof space on a gothic truss construction. *Commun. Sci. Lett. Univ. Zilina* **2013**, *15*, 27–31.
26. Ponechal, R.; Krusinsky, P.; Pisca, P.; Korenkova, R. Simulation and Measurement of Microclimate in Roof Space on a Gothic Truss Construction. In Proceedings of the 27th R-S-P Seminar, Theoretical Foundation of Civil Engineering. MATEC Web Conference, Rostov-on-Don, Russia, 7—21 September 2018; Volume 196, p. 02044.
27. Degelman, L. A Statistically-Based Hourly Weather Data Generator for Driving Energy Simulation and Equipment Design SoftWare for Buildings. In Proceedings of the 2nd International IBPSA Conference Building Simulation, Nice, France, 20–22 August 1991; pp. 592–599.
28. Walton, G.N. Airflow network models for element-based building airflow modeling. *ASHRAE Trans.* **1989**, *95*, 613–620.
29. Zhai, Z.; Chen, Q.; Klems, J.H.; Haves, P. Strategies for Coupling Energy Simulation and Computational Fluid Dynamics Programs. In Proceedings of the 7th International IBPSA Conference Building Simulation, Rio de Janeiro, Brazil, 13–15 August 2001; pp. 59–66.
30. Koronthalyova, O.; Mihalka, P.; Matiašovský, P. Model for complex simulation of HAM-transfer in a single thermal zone building. *Build. Res. J.* **2004**, *52*, 199–217.
31. Moravčíková, K.; Janák, M. Experimental and Theoretical Thermal Analysis of the Transparent Naturally Ventilated Double Skin Facade. In Proceedings of the Junior Scientist Conference 2010, University of Technology, Vienna, Austria, 7–9 April 2010; pp. 373–374.
32. Flack, R.D.; Witt, C.L. Velocity measurements in two natural convection air flows using a laser velocimeter. *J. Heat Transf.* **1979**, *101*, 256–260. [CrossRef]
33. Suchý, L.; Krušinský, P.; Babjaková, Z.; Ďurian, K. *Historical Trusses of the Sacral Buildings in the Region of Turiec*; M. Gibala: Kysucke Nove Mesto, Slovakia, 2008. (In Slovakian)
34. Krušinský, P.; Capková, E. Geometric analysis of the truss above the nave and presbytery of the roman-catholic church in village Bela Dulice. *Adv. Mater. Res.* **2014**, *1020*, 736–740. [CrossRef]
35. Krušinský, P.; Capková, E.; Gocál, J. Comparison of Two Medieval Trusses from the Viewpoint of Geometric and Static Analysis. *Adv. Mater. Res.* **2014**, *1122*, 243–248. [CrossRef]
36. Baharvand, M.; Ahmad, M.H.B.; Safikhani, T.; Majid, R.B.A. DesignBuilder verification and validation for indoor natural ventilation. *J. Basic Appl. Sci. Res.* **2013**, *3*, 182–189.
37. Patankar, S.V. *Numerical Heat Transfer and Fluid Flow*; Taylor and Francis: Boca Raton, FL, USA, 1980.
38. Harris, D.J.; Helwig, N. Solar chimney and building ventilation. *Appl. Energy* **2007**, *84*, 135–146. [CrossRef]
39. Montazeri, H.A. Experimental and numerical study on natural ventilation performance of various multi-opening wind catchers. *BuildEnviron* **2011**, *46*, 370–378. [CrossRef]

40. Hughes, B.R.; Calautit, J.K.; Ghani, S.A. The development of commercial wind towers for natural ventilation: A review. *Appl. Energy* **2012**, *92*, 606–627. [CrossRef]
41. Lau, J.; Niu, J.L. Measurement and CFD simulation of the temperature stratification in an atrium using a floor level air supply method. *Indoor Built Environ.* **2003**, *12*, 265–280. [CrossRef]
42. Katona, Á.L.; Xuan, H.; Elhadad, S.; Kistelegdi, I.; Háber, I. High-resolution CFD and in-situ monitoring based validation of an industrial passive air conduction system (PACS). *Energies* **2020**, *13*, 3157. [CrossRef]